processes

MDPI

Article

Carbon Molecular Sieve Membrane Reactors for Ammonia Cracking

Valentina Cechetto [1,†], Gaetano Anello [1,†], Arash Rahimalimamaghani [1] and Fausto Gallucci [1,2,*]

[1] Inorganic Membranes and Membrane Reactors, Sustainable Process Engineering, Department of Chemical Engineering and Chemistry, Eindhoven University of Technology, De Rondom 70, 5612 AP Eindhoven, The Netherlands; v.cechetto@tue.nl (V.C.); g.anello@tue.nl (G.A.); a.rahimalimamaghani@tue.nl (A.R.)

[2] Eindhoven Institute for Renewable Energy Systems (EIRES), Eindhoven University of Technology, P.O. Box 513, 5600 MB Eindhoven, The Netherlands

* Correspondence: f.gallucci@tue.nl; Tel.: +31-620744662

† These authors contributed equally to this work.

Abstract: The utilization of ammonia for hydrogen storage relies on the implementation of efficient decomposition techniques, and the membrane reactor, which allows simultaneous ammonia decomposition and hydrogen recovery, can be regarded as a promising technology. While Pd-based membranes show the highest performance for hydrogen separation, their applicability for NH_3-sensitive applications, such as proton exchange membrane (PEM) fuel cells, demands relatively thick, and therefore expensive, membranes to meet the purity targets for hydrogen. To address this challenge, this study proposes a solution involving the utilization of a downstream hydrogen purification unit to remove residual ammonia, thereby enabling the use of less selective, therefore more cost-effective, membranes. Specifically, a carbon molecular sieve membrane was prepared on a tubular porous alumina support and tested for ammonia decomposition in a membrane reaction setup. Operating at 5 bar and temperatures ranging from 450 to 500 °C, NH_3 conversion rates exceeding 90% were achieved, with conversion approaching thermodynamic equilibrium at temperatures above 475 °C. Simultaneously, the carbon membrane facilitated the recovery of hydrogen from ammonia, yielding recoveries of 8.2–9.8%. While the hydrogen produced at the permeate side of the reactor failed to meet the purity requirements for PEM fuel cell applications, the implementation of a downstream hydrogen purification unit comprising a fixed bed of zeolite 13X enabled the production of fuel cell-grade hydrogen. Despite performance far from being comparable with the ones achieved in the literature with Pd-based membranes, this study underscores the viability of carbon membranes for fuel cell-grade hydrogen production, showcasing their competitiveness in the field.

Keywords: ammonia decomposition; hydrogen production; carbon molecular sieve membranes; membrane reactor

check for updates

Citation: Cechetto, V.; Anello, G.; Rahimalimamaghani, A.; Gallucci, F. Carbon Molecular Sieve Membrane Reactors for Ammonia Cracking. *Processes* **2024**, *12*, 1168. https://doi.org/10.3390/pr12061168

Academic Editor: Jorge Ancheyta

Received: 5 April 2024
Revised: 30 May 2024
Accepted: 4 June 2024
Published: 6 June 2024

Copyright: © 2024 by the authors. Licensee MDPI, Basel, Switzerland. This article is an open access article distributed under the terms and conditions of the Creative Commons Attribution (CC BY) license (https://creativecommons.org/licenses/by/4.0/).

1. Introduction

Hydrogen (H_2) is widely acknowledged as the ideal energy carrier, holding the potential to replace fossil fuels in several applications and contribute to the decarbonization of the current energy system [1–5]. Nevertheless, the prevailing production methods predominantly rely on non-renewable resources and result in substantial greenhouse gas emissions [6]. In response to this challenge, research is currently exploring alternative and more sustainable methods to produce hydrogen. Although water electrolysis stands out as a promising method for hydrogen production, addressing challenges concerning its distribution and long-term storage is imperative before hydrogen can effectively serve as a pivotal element in the decarbonization of the current energy system.

A promising solution for the sustainable storage, transportation, and on-site production of hydrogen involves the synthesis and decomposition (on the site where H_2 is required) of green ammonia (NH_3) [7–9]. In contrast to hydrogen, ammonia offers advantages in terms of ease of liquefaction, and its existing well-established transportation

infrastructure effectively addresses the challenges associated with hydrogen storage and distribution [8–11]. Furthermore, the carbon-free nature of ammonia, akin to hydrogen, enhances its attractiveness compared to other energy carriers, particularly in scenarios in which the ultimate utilization of hydrogen involves carbon-sensitive applications, such as proton exchange membrane (PEM) fuel cells [10–20]. Nevertheless, the implementation of an NH_3-based energy system requires research efforts to address challenges across the entire value chain of green ammonia, encompassing its production, distribution, and utilization [11]. Particularly, focus should be given to investigating the ammonia decomposition step. Given its inherently energy-intensive nature, attaining high energy efficiencies indeed poses a challenging yet essential requirement for its practical application. The literature reports that a key hindrance to the widespread hydrogen production from ammonia is the development of reliable, efficient, and scalable processes integrating the ammonia decomposition reactor with hydrogen purification systems [21]. In this framework, the membrane reactor has emerged as a promising technology, offering a solution that enables the efficient integration of ammonia decomposition, as per Reaction 1, while simultaneously effecting hydrogen separation, all within a single integrated device [11].

$$NH_3 \leftrightarrow 0.5N_2 + 1.5H_2 \qquad \Delta H_f^o = 45.92 \ \frac{\text{kJ}}{\text{mol}} \tag{1}$$

Moreover, utilizing a membrane reactor has been shown to lower the reactor's operating temperature and increase the reactor's operating pressure compared to conventional systems. This results in higher energy efficiency due to the lower temperature conditions and improved reactor compactness thanks to the elevated pressure levels [10,15,20,21]. The selective separation of hydrogen from the reaction zone, which is favored at high pressure, enhances, in fact, the reaction rates and shifts the reaction equilibrium towards the formation of reaction products, resulting in increased feedstock conversions.

Hydrogen production via ammonia decomposition has been experimentally studied in numerous studies available in the literature [13,22–38] and the best performance in terms of ammonia conversion, hydrogen recovery, and purity has been achieved using a Ru-based catalyst to promote ammonia decomposition and Pd-based membranes for hydrogen separation [11]. This can be attributed to the outstanding permeance and selectivity towards hydrogen separation of Pd-based membranes compared to other types of membranes. However, considering the potential use of the produced hydrogen for PEM fuel cell applications, ensuring compliance with the residual ammonia limit required for the proper functioning of the device has proven to be challenging. Hydrogen meeting the fuel cell-grade standard with residual ammonia concentrations below 0.1 ppm—as indicated in the standard ISO 14687:2019 [39]—may in fact require relatively thick, and therefore expensive, Pd-based membranes. In one of our previous studies [25], we achieved, for example, the production of hydrogen containing residual ammonia concentrations below 0.75 ppm by implementing a 195 mm long membrane with a selective layer with a thickness of ~6–8 µm. This result was obtained while performing ammonia decomposition over a bed of 250 g of 2 wt.% Ru/Al_2O_3 at 500 °C, with a pressure difference across the membrane of 1 bar, under a feed flow rate of 500 ml_N/min. Similarly, Cerrillo et al. [35] obtained NH_3-free hydrogen while performing ammonia decomposition over a Co-based catalyst in a packed bed membrane reactor using a 186 mm long Pd-Au alloy membrane with an 8 µm thick selective layer. Various studies in the literature showed that a more economically competitive alternative to circumvent this challenge, while aiming to achieve the desired level of hydrogen purity, involves the purification of hydrogen from residual ammonia in a dedicated purification unit downstream of the membrane reaction. Despite the complexity it introduces to the system, this alternative may be considered advantageous from both economic and energy perspectives, as the inclusion of a hydrogen purification stage provides the opportunity to produce ultra-pure hydrogen while operating at lower reactor temperatures and using thinner membranes, thereby reducing energy consumption and costs. Sitar et al. [37] demonstrated that residual ammonia impurities in the hydrogen stream can be diminished from ~1000 ppm to values below 0.025 ppm by employing clinoptilolite zeolite as an adsorbent material. We

also demonstrated that hydrogen with a residual ammonia concentration below 0.75 ppm can be produced even at temperatures as low as 450 °C using a Pd-Ag membrane with an ~1 μm thick selective layer implementing a bed of zeolite 13X at ambient conditions downstream of the membrane reactor [25]. The findings of these studies show that it is possible to decouple the production of hydrogen-containing residual ammonia within the fuel cell limits from the membrane's separation performance. In other words, this translates into the fact that fuel cell-grade hydrogen can be produced in a membrane reactor by not only implementing highly selective membranes, such as Pd-based membranes, but also adopting membranes with lower selectivity towards hydrogen compared to Pd-based ones.

In this study, we, therefore, propose the adoption of this approach, coupled with the integration of carbon molecular sieve membranes into the membrane reactor for hydrogen recovery from ammonia. Carbon membranes are in fact less expensive compared to Pd-based membranes; thus, the costs associated with the reaction unit are reduced upon their utilization. Carbon molecular sieve membranes have already been evaluated for ammonia decomposition in the study conducted by Jiang et al. [34]. The authors performed ammonia decomposition over a $Ru/Y/K/Al_2O_3$ catalyst with different types of membranes and demonstrated that the residual ammonia concentration in the hydrogen produced strongly depends on the separation performance of the membrane. Specifically, carbon molecular sieve membranes were proven to have significantly lower performance compared to Pd-Ag membranes during ammonia decomposition: the decomposition of an ammonia flow of 250 mL/min over 3 g of catalyst at 450 °C and 7 bar resulted in the production of hydrogen with residual NH_3 concentrations of ~50 ppm when implementing an 80 mm long and 1.8 μm thick Pd-Ag membrane, whereas under similar operating conditions, the residual NH_3 concentrations were measured to be ~10,000 ppm when implementing a 220 mm long and 0.9 μm thick carbon molecular sieve membrane. While a comparison between the performance of carbon molecular sieve membranes and Pd-based membranes is, therefore, available in the literature, to the best of our knowledge, the applicability of carbon molecular sieve membranes for the production of fuel cell-grade hydrogen has not been demonstrated yet. In this study, a carbon molecular sieve membrane was therefore prepared, characterized, and tested for ammonia decomposition application in a fixed bed membrane reaction configuration, implementing downstream a hydrogen purification unit from ammonia.

2. Material and Methods

2.1. Membrane Preparation

The carbon membrane employed in this study was prepared starting from an asymmetric tubular porous alumina support with subsequent coating, polymerization, and carbonization under controlled conditions. In detail, the preparation procedure (Figure 1), for which the chemicals listed in Table 1 have been used, was carried out according to the following steps:

1. **Support preparation.** The support was prepared starting from an asymmetric porous alpha alumina tube with an outer diameter (OD) of 10 mm, an inner diameter (ID) of 7 mm, and an external layer with an average pore size of about 100 nm (Rauschert GmbH, Steinbach am Wald, Germany). As reported in a previous study [40], the porous alumina tube is connected on one side to a dense alumina cap and on the other side to a dense alumina tube through appropriate glass sealing. This allows one of the sides to be completely closed, whereas the other one is open to ensure the gas outlet, resulting in a dead-end configuration.
2. **Polymeric precursor synthesis**. Along with the support preparation, another preliminary step to the fabrication of the carbon membrane is the synthesis of the oligomer employed in the dipping solution. The resin is synthesized via an acid-catalyzed phenol–formaldehyde condensation, with the following procedure [40,41]. Phenol (69 g) was gradually melted at 60 °C in a four-necked round-bottom flask equipped with a Graham condenser. Upon liquefying, oxalic acid (1.5 g) was added to the

solution, and the temperature was increased up to 90 °C while adding formaldehyde solution (54 g) to the flask at a rate of 2 mL/min. After 8 h, the obtained product was washed and separated by centrifugation (three cycles of 15 min at 4400 rpm and 10 °C). Finally, the obtained oligomer was dried under vacuum at 50 °C for 24 h.

3. **Dipping Solution Preparation.** Then, the dipping solution was prepared by dissolving the Novolac synthesized (30 g) in N-Methyl-2-Pyrrolidone (83.2 g) with aluminum acetylacetonate (0.8 g) as an additive [40]. A high-shear mixer (Thinky ARE-250, Tokyo, Japan) was employed to ensure the efficient mixing of the chemicals at 2000 rpm for two cycles with a duration of 30 min each. Next, formaldehyde (1.6 g) was added with a subsequent mixing step, again at 2000 rpm for 30 min. Finally, oxalic acid (0.4 g) was added to the solution and mixed at 2000 rpm for an additional 30 min.
4. **Dip Coating.** The support was dip-coated by a laboratory-made automated system where the machine lowers and raises the support inside a graduated cylinder containing the dipping solution.
5. **Polymerization.** Once the dip coating has been completed, the coated support is dried-polymerized in a laboratory-made rotary oven at 80 °C for 24 h. The coated support is connected to a rotating mount while drying to ensure a more homogeneous active layer thickness. Furthermore, nitrogen gas was employed to provide an inert atmosphere.
6. **Carbonization.** Finally, the polymeric layer on the porous support underwent carbonization in a tubular three-zone oven (Nabertherm R 170/1000/1, Lilienthal, Germany). A heating rate of approximately 1 °C/min was applied until reaching a temperature of about 800 °C, where it was held for 4 h. Throughout the carbonization step, a nitrogen flow of about 3 L/min was applied to avoid carbon combustion.

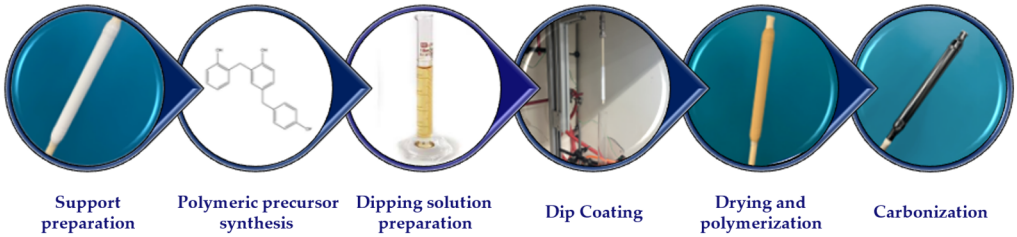

Figure 1. Schematic of the membrane preparation process.

Table 1. List of chemicals used for the membrane's synthesis.

Chemical	CAS n.	Purity	Brand	Supplier
Formaldehyde solution	50-00-0	37.0%	Sigma Aldrich	VWR International BV
Phenol	108-95-2	99.9%	Sigma Aldrich	VWR International BV
N-Methyl-2-Pyrrolidone	872-50-4	99.5%	Sigma Aldrich	Merck Life Science NV
Aluminum acetylacetonate	13963-57-0	99.9%	Sigma Aldrich	Merck Life Science NV
Oxalic acid	144-62-7	98.0%	Sigma Aldrich	VWR International BV

2.2. Membrane Characterization

The pore size distribution measurements of the fabricated carbon membrane were performed with a laboratory-made capillary condensation perm-porometer [41], of which details are given in Appendix A.

2.3. Experimental Setup

The carbon molecular sieve membrane, whose preparation procedure has been outlined in the previous section, was tested in an experimental setup specifically designed for ammonia decomposition. The setup comprises four main modules: (1) the feed module, (2) the permeation module, (3) the hydrogen purification module, and (4) the retentate/permeate analysis module. In the feed module, mass flow controllers (Bronkhorst, Ruurlo, The Netherlands) regulate the desired flow rate of feed gases (NH_3, H_2, and N_2) to the system. The permeation module includes a stainless-steel vessel with an inner

diameter of 4.5 cm and a length of 28 cm, in which the membrane is connected to the flange, positioned in the middle of the reactor, and fully immersed in a packed-bed of 250 g of commercial (2 wt.%) Ru/Al_2O_3 catalyst in pelletized form (3 mm) (Alfa Aesar) during ammonia decomposition. The reactor's inlet is equipped with a porous stainless-steel plate to guarantee even gas distribution, and the reactor's freeboard is configured in a conical shape to decrease the gas velocity and mitigate the potential for the escape of catalyst particles during the experimental campaign. Moreover, the pressure of the system is controlled by means of a back pressure regulator, and, given the endothermic nature of the ammonia decomposition reaction, an electrical split oven is used to supply heat to the reactor. The hydrogen purification module employs a bed of zeolite 13X at ambient conditions for NH_3 removal from the permeate stream, whereas the retentate/permeate analysis module comprises the instrumentation for measuring permeation flux through the membrane and the composition of both retentate and permeate streams. Specifically, a film-flow meter (Horiba Stech Co. Ltd., Kyoto, Japan) and a mass flow meter (Bronkhorst, Ruurlo, The Netherlands) are used to quantify the permeation flux through the membrane, a micro gas chromatograph (CP-4900 Varian Inc., CA, USA) is used to measure the composition of the retentate and permeate streams leaving the reactor, and a Fourier-transform infrared spectrometer (FTIR) (Shimadzu Corp., Kyoto, Japan) with a 5 m gas cell (Specac Ltd., Orpington, United Kingdom) and an mercury-cadmium-telluride (MCT) detector is employed to measure the residual ammonia concentration of the permeate stream leaving the hydrogen purification module. This instrument is capable of accurately determining residual concentrations of ammonia as low as 0.75 ppm. The permeate and retentate streams leaving the analysis module are directed to a water absorption unit to prevent the release of the residual NH_3 traces into the atmosphere, which is eventually vented.

2.4. Experimental Method

After completing the membrane preparation procedure, the carbon molecular sieve membrane underwent sealing and testing in helium/ethanol to ensure the absence of any undesired leakages from both the sealings and the membrane surface. Once confirmed leak-free, the membrane was installed in the reactor. The reactor was gradually heated to 500 °C at a rate of 2 °C/min under a nitrogen (N_2) atmosphere. Subsequently, the system was transitioned to a hydrogen (H_2) atmosphere until steady permeation was attained. Single gas (H_2, N_2, and NH_3) and binary mixtures (H_2/N_2) permeation tests were subsequently performed.

Gas permeation measurements for pure H_2, N_2, and NH_3 were conducted across temperatures ranging from 400 °C to 500 °C, with pressure differences across the membrane ranging between 1 and 5 bar, while maintaining atmospheric conditions on the permeate side of the membrane. Temperature changes between the measurements at different temperatures were carried out in an N_2 atmosphere under a heating/cooling rate of 2 °C/min. From the gas permeation measured, the H_2, N_2, and NH_3 permeances, as well as the ideal H_2/N_2 and H_2/NH_3 ideal perm-selectivities of the membrane, were then calculated.

H_2/N_2 permeation tests were performed with the aim of assessing if the presence of N_2 next to H_2 in the feed stream has an influence on the gas permeation through the membrane. A H_2/N_2 mixture containing H_2 concentrations ranging between 50 vol.% and 95 vol.% was fed to the reactor at 450 °C for a pressure difference across the membrane ranging between 1 and 5 bar. The permeate side of the membrane was kept at atmospheric conditions.

The reactor was then cooled down in an N_2 atmosphere at a cooling rate of 2 °C/min and, once the room temperature was achieved, the catalyst was introduced into the reactor. Subsequently, the reactor was heated up in the N_2 atmosphere, and permeation tests under reactive conditions were performed. Specifically, ammonia decomposition was performed at 450, 475, and 500 °C, keeping the retentate and permeate sides of the membrane at 5 bar and atmospheric conditions, respectively. At each temperature, a flow rate of 0.5 l_N/min of pure NH_3 was fed to the reactor, the operating pressure was varied, and the reaction performance was monitored until steady-state operation was achieved. The gas permeation through the membrane, the composition of the streams leaving at the permeate and retentate

sides of the membrane, and the NH_3 concentration in the permeate stream downstream of the hydrogen cleanup unit were then measured 5 times. Subsequently, the NH_3 conversion (ξ_{NH_3}) and the H_2 recovery (HR) were calculated according to Equations (2) and (3), respectively. The values of NH_3 concentration in the permeate, NH_3 conversion, and H_2 recovery reported in this study for a specific combination of experimental conditions represent the average of five measured or calculated values.

$$\xi_{NH_3} = \frac{NH_{3,\,in} - NH_{3,\,out}}{NH_{3,\,in}} \tag{2}$$

$$HR = \frac{H_{2,\,permeated}}{1.5 \cdot NH_{3,\,in}} \tag{3}$$

3. Results and Discussion

In Figure 2, the pure hydrogen permeation flux (a) and the hydrogen permeance through the membrane (b) as a function of the transmembrane pressure difference across the membrane for different temperatures are represented. As illustrated in Figure 2a, the hydrogen permeation flux through the membrane increases with increasing pressure. This is due to the higher driving force for separation available when pressure increases. Moreover, the increase in hydrogen permeance with temperature, which is visible in Figure 2b, indicates the dominance of activated transport mechanisms such as molecular sieving and surface diffusion. The negative slope of hydrogen permeation as a function of pressure indicates the negligible contribution of viscous flow through the membrane and, therefore, the absence of defects on the membrane's surface [42]. This result is also confirmed by the fact that nitrogen permeation through the membrane was not observed in any of the tested conditions.

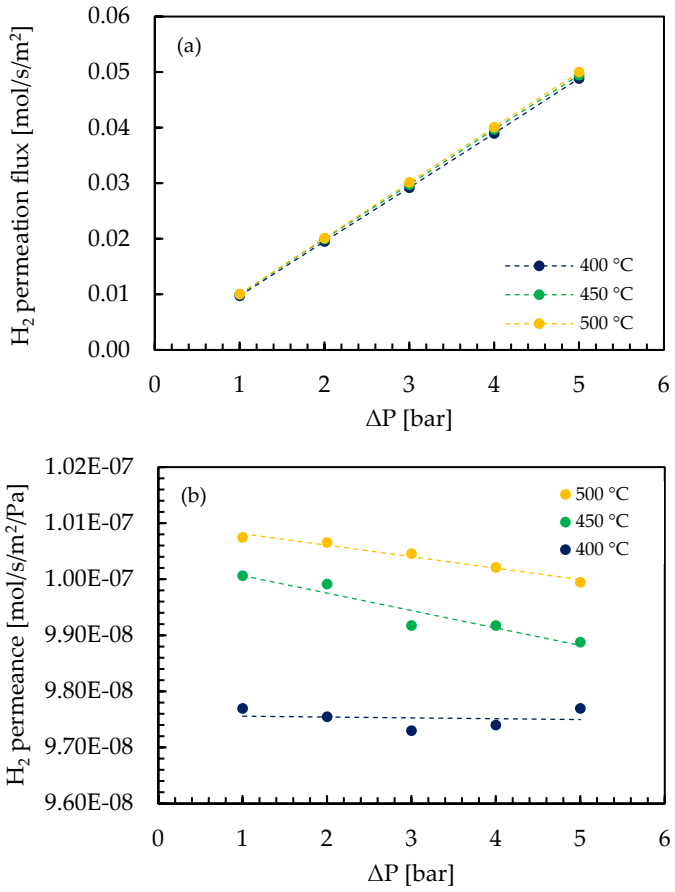

Figure 2. Hydrogen permeation flux (**a**) and permeance (**b**) through the membrane as a function of the pressure difference across the membrane at different temperatures.

The measured hydrogen, nitrogen, and ammonia permeances at 400, 450, and 500 °C, with a pressure difference of 1 bar across the membrane, are outlined in Table 2, along with the corresponding H_2/N_2 and H_2/NH_3 ideal perm-selectivity. Additionally, in Figure 3, the permeance of NH_3, H_2, and N_2 at different temperatures is depicted as a function of their kinetic diameter. Since nitrogen permeation through the membrane was not observed, in Table 3 and Figure 3, N_2 permeance and H_2/N_2 selectivity are reported under the assumption of the worst-case scenario. This entails considering the nitrogen permeation flow rate through the membrane to be as low as the low detection limit of the flow meters used for nitrogen permeation measurement (0.2 mL/min). Hydrogen is the gas showing the highest permeance, and this can be explained by analyzing the pore size distribution of the membrane, given in Figure 4. Here, it is, in fact, shown that most of the pores are bigger than the kinetic diameter of hydrogen (0.289 nm), indicating that hydrogen permeation through the membrane is promoted. Nitrogen permeation through the membrane is, on the other hand, less favored since only about 26% of the pores show a bigger size compared to their kinetic diameter. This permeance pattern, which is consistent with findings of other studies previously reported in the literature [43–45], confirms the contribution of molecular sieving to the permeation mechanism through the membrane observed in Figure 2. As far as ammonia concerns, despite its lower kinetic diameter compared to the one of hydrogen, it shows a lower permeance compared to the one of hydrogen. The main reason for this lies in the contribution of molecular sieving to the permeation mechanism. Ammonia permeation can in fact only take place through those pores that have a larger size compared to their kinetic diameter (0.260 nm) and is therefore inhibited through about 24% of the pores. Moreover, a similar behavior of permeation compared to hydrogen has been observed in the literature for helium (He), which indeed has the same kinetic diameter as ammonia. As this behavior has been ascribed to the higher adsorption affinity of hydrogen in carbon membranes compared to helium as well as the smaller cross-section diameter of hydrogen that results in lower resistance to gas transport through the pores by molecular sieving mechanisms [46], the same explanation might justify the trend of ammonia permeation compared to the one of hydrogen experienced in this study.

Table 2. H_2, N_2, and NH_3 permeance and ideal H_2/N_2 and H_2/NH_3 perm-selectivity of the membrane used in this study at 450 °C and 1 bar.

Temperature [°C]	H_2 Permeance [mol/s/m^2/Pa]	N_2 Permeance [mol/s/m^2/Pa]	NH_3 Permeance [mol/s/m^2/Pa]	H_2/N_2 Ideal Perm-selectivity [-]	H_2/NH_3 Ideal Perm-selectivity [-]
400	9.8×10^{-8}	$<5.9 \times 10^{-10}$	6.0×10^{-9}	>165	16
450	1.0×10^{-7}	$<5.9 \times 10^{-10}$	6.2×10^{-9}	>169	16
500	1.0×10^{-7}	$<5.9 \times 10^{-10}$	8.1×10^{-9}	>170	12

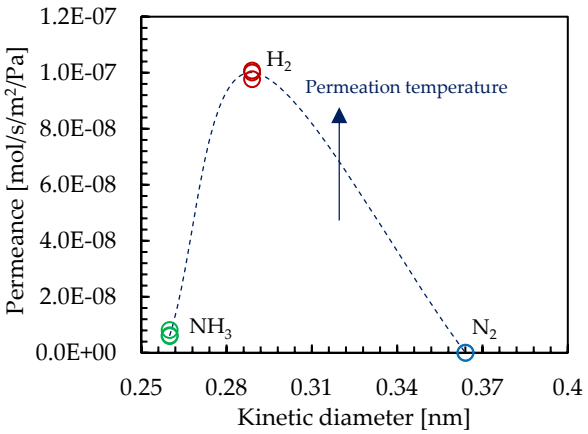

Figure 3. Permeance of NH_3, H_2, and N_2 at 400, 450, and 500 °C and 1 bar pressure difference across the CMSM used in this study as a function of their kinetic diameter.

Table 3. NH_3 conversion, H_2 recovery, and NH_3 concentration in the permeate at different ammonia decomposition reaction temperatures.

Temperature [°C]	NH_3 Conversion [%]	H_2 Recovery [%]	NH_3 Concentration in the Permeate [%]
450	91.38 ± 0.29	8.15 ± 0.01	4.01 ± 0.08
475	97.87 ± 0.18	8.98 ± 0.13	1.30 ± 0.05
500	98.49 ± 0.05	9.84 ± 0.02	0.59 ± 0.00
Reaction pressure of 5 bar and NH_3 feed flow rate of 0.5 l_N/min.			

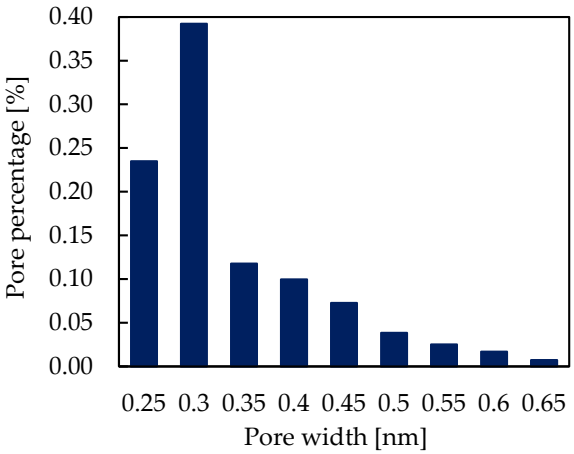

Figure 4. Pore size distribution of the supported carbon membrane used in this study measured via perm-porometry.

In Figure 5, the gas flow rate through the membrane is depicted as a function of the hydrogen partial pressure difference across the membrane for both pure H_2 and H_2/N_2 feed mixtures with hydrogen concentrations ranging from 50 vol.% to 90 vol.%. As it is possible to see, at a given hydrogen partial pressure difference across the membrane, hydrogen recovery is independent of the hydrogen concentration in the feed mixture. These results, which are in line with other studies available in the literature [47], show that carbon membranes are not subject to mass transfer limitations and that no reduction in the hydrogen permeation flux through the membrane is expected during ammonia decomposition compared to operation in a pure hydrogen environment.

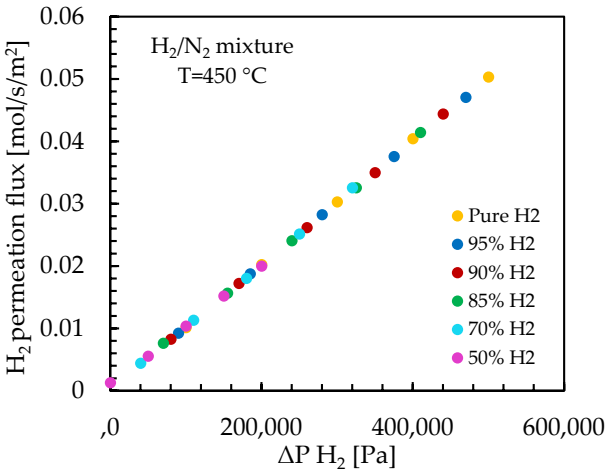

Figure 5. Hydrogen flow rate at different hydrogen partial pressure differences across the CMSM for pure hydrogen and binary H_2/N_2 mixtures with different compositions.

After the performance of the binary mixture permeation tests, single gas permeation tests have been repeated in order to assess if high operation temperatures have an impact on the separation performance of the membrane. The hydrogen, nitrogen, and ammonia permeation fluxes through the membrane were measured to be similar to the ones measured before the performance of binary mixture permeation tests, showing that the membrane separation properties were stable during operation at high temperatures. Pure hydrogen and nitrogen permeation tests were then repeated after the catalyst introduction in the reactor and, specifically, following the cooling and re-heating of the reactor prior to executing permeation tests under reacting conditions. The hydrogen permeation displayed a marginal increment, while nitrogen, which had previously remained undetectable during single gas permeation tests, became discernible. Particularly, for a pressure difference across the membrane of 1 bar, the H_2 and N_2 permeances were measured to be 1.0×10^{-7} and 3.8×10^{-9}, respectively, at 450 °C, resulting in an ideal H_2/N_2 perm-selectivity of 26; at 500 °C, the H_2 and N_2 permeances were measured to be 1.1×10^{-7} and 3.7×10^{-9}, respectively, resulting in an ideal H_2/N_2 perm-selectivity of 29. A postmortem helium/ethanol leakage test revealed that no defects were formed on the membrane surface, but that the increase in nitrogen permeation should be attributed to the degradation of the membrane's sealing that occurred during the cooling and re-heating phases of the reactor.

The performance of the membrane reactor for ammonia decomposition operated at 5 bar and under a feed flow rate of 0.5 ml_N/min of pure ammonia is reported in Table 3 and Figure 6 for different operating temperatures. In agreement with findings in the existing literature [13,22–26,28,29,33,35,36], a temperature increase yields an increase in both NH_3 conversion and H_2 recovery. A higher temperature favors, in fact, both the ammonia decomposition kinetics and thermodynamics, leading to enhanced NH_3 conversion. This brings NH_3 conversion closer to the calculated thermodynamic equilibrium conversion (without hydrogen separation membrane) for temperatures higher than 475 °C. Simultaneously, as NH_3 conversion increases, so does the hydrogen partial pressure in the reactor. This, in turn, results in a higher driving force for hydrogen separation and ultimately into a higher recovery. From Table 3 and Figure 6, it is noteworthy that a temperature increase has also a positive impact on hydrogen purity; as temperatures increase, the residual NH_3 concentration in the permeate decreases. These results, which align with the results of our previous studies [25,26], can be attributed to the fact that a lower amount of NH_3 is available for separation when temperature increases due to a higher NH_3 conversion. Although these results show that the hydrogen produced at the permeate side of the membrane reactor may not be directly used for systems requiring ultra-pure hydrogen as feedstock, the residual NH_3 concentration of the permeate stream was measured to be below 0.75 ppm downstream of the purification unit. These results, which are consistent with other studies documented in the literature [14,18,25,48–51], demonstrate that commercially available adsorbent materials are effective in reducing the residual ammonia concentration in the produced hydrogen stream to levels suitable for applications in PEM fuel cells.

Table 4 presents a comparison between the results achieved in this study, the results obtained in our previous investigations using ceramic and metallic supported Pd-Ag membranes [25,27], and the outcomes of the study by Jiang et al. [34] involving a carbon molecular sieve membrane. The H_2 recovery and the NH_3 conversion achieved during ammonia decomposition follow a trend that is dependent on the hydrogen permeation properties of the membranes. Particularly, the lower hydrogen permeance and length of the membrane used in this study result in a lower H_2 recovery and NH_3 conversion compared to the ones achieved with Pd-based membranes in our previous studies. Carbon membranes show, in fact, lower hydrogen permeance compared to Pd-based membranes due to the different transport mechanisms governing permeation. The different permeation mechanisms through the membrane also justify the significantly lower selectivity towards hydrogen achieved in this study compared to the one achieved with Pd-Ag membranes. While, in fact, the selective layer of Pd-based membranes is dense and hydrogen permeation takes place because palladium acts as a catalyst for hydrogen splitting, the permeation

of gases through a carbon membrane, being its selective layer porous, mainly depends on the pore size distribution, which also enables contaminant gases to permeate in cases where pores with a diameter larger than the contaminant's kinetic diameter are available. Accordingly, the residual ammonia concentration in the hydrogen produced in this study is significantly higher compared to the results achieved by implementing Pd-based membranes for hydrogen separation. These results are well in agreement with the findings by Jiang et al. [34], who observed an increase in the residual NH_3 concentration in the hydrogen stream from ~50 to ~10,000 ppm when replacing in their system for ammonia decomposition an 80 mm long 1.8 µm thick Pd-Ag membrane with a 220 mm long 0.9 µm thick carbon molecular sieve membrane.

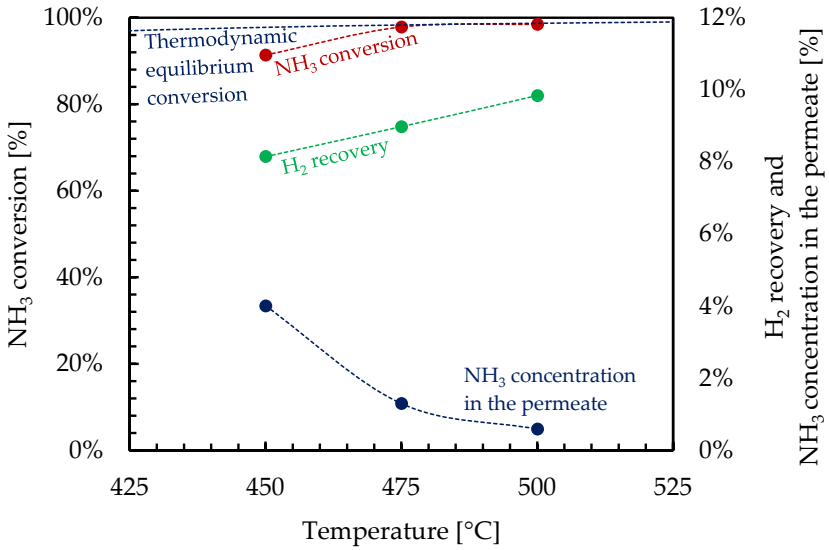

Figure 6. NH_3 conversion, H_2 recovery, and residual NH_3 concentration in the permeate achieved in the membrane reactor at 450, 475, 500 °C, 5 bar(a), under a feed flow rate of 0.5 l_N/min of pure NH_3.

Table 4. Comparison between the experimental results achieved in this study and in the studies of Cechetto et al. [25,27] and Jiang et al. [34].

	Cechetto et al. [25]	Cechetto et al. [27]	Jiang et al. [34]	This Study
		Membrane		
Membrane configuration	Supported tubular double-skinned Pd-based	Supported tubular Pd-based	Supported tubular carbon-based	Supported tubular carbon-based
Support	Al_2O_3	Hastelloy X	N/A	Al_2O_3
Selective layer composition	Pd-Ag	Pd-Ag	Carbon	Carbon
Selective layer thickness [µm]	~ 6–8	~ 6–8	~ 0.9	< 1
Membrane length [mm]	195	90	220	80
Membrane area [cm^2]	85.8	39.6	34.1	25.1
H_2 permeance at 450 °C and 1 bar(g) [mol/s/m^2/Pa]	1.2×10^{-6}	6.6×10^{-7}	N/A	1.0×10^{-7}
H_2/N_2 ideal perm-selectivity at 450 °C, 1 bar(g) [mol/s/m^2/Pa]	68,960	5,890	N/A	26

Table 4. *Cont.*

	Cechetto et al. [25]	Cechetto et al. [27]	Jiang et al. [34]	This Study
		Reactor operating conditions		
Catalyst	Ru/Al_2O_3 (2 wt.%) 250 g	Ru/Al_2O_3 (2 wt.%) 250 g	$Ru/Y/K/Al_2O_3$ (3 wt.%) 3 g	Ru/Al_2O_3 (2 wt.%) 250 g
Reaction pressure [bar]	5	5	7	5
Permeate pressure [bar]	1	1	1	1
NH_3 feed flow rate [ml_N/min]	500	500	250	500
GHSV [$ml/(g_{cat}\ h)$]	120	120	5000	120
Temperature [°C]		**NH_3 conversion [%]**		
450	99.7	98.2	98.9	91.4
475	99.8	99.2	N/A	97.9
500	99.8	99.3	N/A	98.5
Temperature [°C]		**H_2 recovery [%]**		
450	87.8	55.5	93.7	8.2
475	88.9	60.7	N/A	9.0
500	88.9	62.9	N/A	9.8
Temperature [°C]		**NH_3 concentration in the permeate**		
450	11.8	N/A	<10,000	40,000
475	6.1	N/A	N/A	13,000
500	1.6	N/A	N/A	6000

From Table 4, it is possible to observe that Jiang et al. obtained much higher NH_3 conversion and hydrogen recovery as well as lower residual NH_3 concentrations compared to the results obtained in this study. Although the results have been achieved at different operating conditions, which renders a direct quantitative comparison between the two sets of outcomes a non-trivial task, better results in this study could be achieved through the optimization of the installed membrane area as compared to the amount of catalyst used and of the residence time of ammonia in the reactor.

In all the scenarios presented in Table 4, fuel cell-grade hydrogen containing residual NH_3 concentrations < 0.1 ppm could not be achieved at the reactor outlet. This implies that the hydrogen produced in these systems may not be directly used as feedstock for PEM fuel cells. In one of our previous studies [25] as well as in the study authored by Sitar et al. [37], the addition of a hydrogen purification stage downstream of the membrane reactor implementing Pd-based membranes was demonstrated to be an effective solution to produce fuel cell-grade hydrogen. Similar results have been achieved in this study by implementing downstream a reactor, a carbon membrane, and an adsorption unit for residual NH_3 removal consisting of a fixed bed of zeolite 13X. In light of these results, this study demonstrates that carbon membranes, despite the requirement for scaling up membrane length and potential enhancement in their hydrogen permeation properties, represent a competitive alternative to Pd-based membranes for the production of fuel cell-grade hydrogen. Carbon membranes are, in fact, less expensive compared to Pd-based membranes; thus, the costs associated with the reaction unit are reduced upon their utilization.

4. Conclusions

In this study, a carbon molecular sieve membrane has been prepared on a tubular porous alumina support and subsequently tested for hydrogen separation during ammonia decomposition. In agreement with the results reported in the literature, the H_2/N_2 mixture permeation tests demonstrated that the membrane does not suffer from mass transfer limitation phenomena during permeation. No reduction in the hydrogen permeation flux through the membrane is therefore to be expected during ammonia composition compared

to operation in a pure hydrogen environment. During the experimental tests under an ammonia decomposition environment, > 90% NH_3 conversion rate was achieved in the entire range of operating conditions investigated, and NH_3 conversion approaching the conventional thermodynamic equilibrium conversion was achieved at a temperature of 475 °C. The hydrogen recovered from ammonia through the carbon membrane amounts to 8.2–9.8% in the temperature range between 450 and 500 °C. Despite this being a very low value for hydrogen recovery, better results could be achieved in this study through the optimization of the installed membrane area as compared to the amount of catalyst used and the residence time of ammonia in the reactor. While hydrogen produced at the permeate side of the reactor could not meet the specification on hydrogen purity imposed for PEM fuel cell application, fuel cell-grade hydrogen production could be achieved by implementing a hydrogen purification unit consisting of a fixed bed of zeolite 13X downstream the membrane reactor. Therefore, while the hydrogen separation performance of carbon molecular sieve membranes is far from comparable with the ones achievable with Pd-based membranes, this study demonstrates that carbon membranes can still be regarded as a competitive alternative to Pd-based membranes for the production of fuel cell-grade hydrogen. Carbon membranes are in fact less expensive compared to Pd-based membranes; thus, the costs associated with the reaction unit are reduced upon their utilization. However, it must be mentioned that when designing a membrane reactor-assisted NH_3-to-H_2 system, it should be taken into account that the different separation performances of the implemented membranes affect the ultimate design of the system. If, in fact, the implementation of carbon membranes can result in a decrease in the costs associated with the reaction unit, their lower selectivity towards hydrogen will likely result in the need for bigger units for residual NH_3 removal and, in the case of the PEM fuel cell, for on-board application and for residual N_2 separation units. The economic optimum of the system is therefore given by the design solution, which allows the minimization of the sum of the costs associated with both the reaction unit and the hydrogen purification unit.

Author Contributions: Conceptualization, V.C. and G.A; methodology, V.C. and G.A.; investigation, V.C.; resources, G.A.; data curation, V.C., G.A. and A.R.; writing—original draft preparation, V.C. and G.A. (these authors contributed equally to this work); writing—review and editing, F.G.; visualization, V.C. and G.A.; supervision, F.G.; project administration, F.G.; funding acquisition, F.G. All authors have read and agreed to the published version of the manuscript.

Funding: This study is funded by the European Commission under agreement 101112118.

Data Availability Statement: Data are contained within the article.

Acknowledgments: The views and opinions expressed are, however, those of the author(s) only and do not necessarily reflect those of the European Union. Neither the European Union nor the granting authority can be held responsible for them.

Conflicts of Interest: The authors declare no conflict of interest.

Appendix A. Membrane Characterization: Perm-Porometry Setup

The perm-porometry analysis method is based on the capillary condensation of liquids in porous media. From the Kelvin equation (Equation (A1)), it is known that, in a capillary, the vapor condensation takes place at lower pressures than the saturated vapor pressure. Moreover, the lower the characteristic dimensions of the capillary, the lower the pressure at which the abovementioned phenomenon will happen. Thus, it is possible to send to the porous membrane a mixture of a non-condensable gas and a condensable vapor, and then the permeation rate of the non-condensable gas can be measured as a function of the vapor pressure of the condensable vapor. This procedure allows for the estimation of the pore size distribution as the permeation of the non-condensable gas in larger pores is hindered by larger vapor pressures [52–54].

$$R \cdot T \cdot ln\left(\frac{p_V}{p_s}\right) = 2 \cdot \nu \cdot \frac{\sigma \cdot cos\theta}{r_p} \quad \text{(A1)}$$

First, the membrane underwent a 24 h drying procedure under a nitrogen atmosphere at 300 °C and at a pressure difference of 5 bar between retentate and permeate to eliminate any condensed water from the pores. Subsequently, the system was cooled to room temperature, and helium was employed as a non-condensable gas to measure the permeance in the dry membrane. Later, condensable vapor was gradually introduced by injecting demi water into the helium stream to occlude the pores of the fabricated membranes at 70 °C and at a pressure difference of 2 bar. The pore size was calculated according to Kelvin's equation, where R is the universal gas constant, T is the temperature of the system, p_v is the vapor pressure, p_s is the saturated vapor pressure, v is the molar volume of the liquid, σ is the vapor-liquid surface tension, θ is the contact angle, and r_p is the pore radius. Of note, the application of the Kelvin equation for pores lower than 2 nm can lead to inaccuracies [53]. However, the vapor pressure reduction described by the Kelvin equation still occurs for considerably smaller pores; therefore, it is still possible to assign a quantitative measure [55].

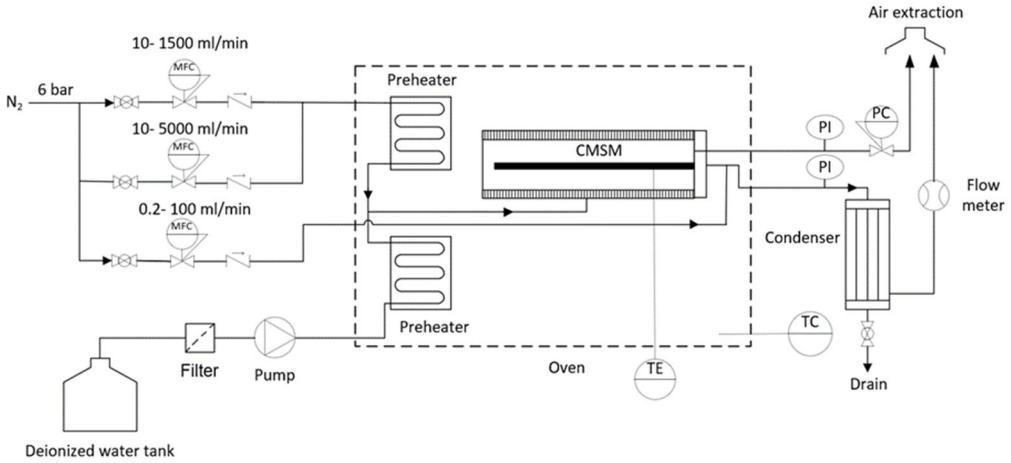

Figure A1. Schematic representation of the perm-porometer designed to measure the pore size distribution of tubular carbon membranes using water as an adsorbate and helium as an inert gas.

References

1. Dell, R.; Bridger, N. Hydrogen—The ultimate fuel. *Appl. Energy* **1975**, *1*, 279–292. [CrossRef]
2. Rosen, M.A.; Koohi-Fayegh, S. The prospects for hydrogen as an energy carrier: An overview of hydrogen energy and hydrogen energy systems. *Energy Ecol. Environ.* **2016**, *1*, 10–29. [CrossRef]
3. Abe, J.O.; Popoola, A.P.I.; Ajenifuja, E.; Popoola, O.M. Hydrogen energy, economy and storage: Review and recommendation. *Int. J. Hydrogen Energy* **2019**, *44*, 15072–15086. [CrossRef]
4. Bockris, J.O. The hydrogen economy: Its history. *Int. J. Hydrogen Energy* **2013**, *38*, 2579–2588. [CrossRef]
5. Johnston, B.; Mayo, M.C.; Khare, A. Hydrogen: The energy source for the 21st century. *Technovation* **2005**, *25*, 569–585. [CrossRef]
6. International Energy Agency. The Future of Hydrogen. Paris, 2019. Available online: https://www.iea.org/reports/the-future-of-hydrogen (accessed on 2 January 2024).
7. Lan, R.; Tao, S. Ammonia as a Suitable Fuel for Fuel Cells. *Front. Energy Res.* **2014**, *2*, 110206. [CrossRef]
8. Lamb, K.E.; Dolan, M.D.; Kennedy, D.F. Ammonia for hydrogen storage; A review of catalytic ammonia decomposition and hydrogen separation and purification. *Int. J. Hydrogen Energy* **2019**, *44*, 3580–3593. [CrossRef]
9. Klerke, A.; Christensen, C.H.; Nørskov, J.K.; Vegge, T. Ammonia for hydrogen storage: Challenges and opportunities. *J. Mater. Chem.* **2008**, *18*, 2304–2310. [CrossRef]
10. Valera-Medina, A.; Xiao, H.; Owen-Jones, M.; David, W.I.F.; Bowen, P.J. Ammonia for power. *Prog. Energy Combust. Sci.* **2018**, *69*, 63–102. [CrossRef]
11. Cechetto, V.; Di Felice, L.; Gallucci, F. Advances and Perspectives of H_2 Production from NH_3 Decomposition in Membrane Reactors. *Energy Fuels* **2023**, *37*, 10775–10798. [CrossRef]
12. Li, G.; Kanezashi, M.; Tsuru, T. Highly enhanced ammonia decomposition in a bimodal catalytic membrane reactor for CO -free hydrogen production. *Catal. Commun.* **2011**, *15*, 60–63. [CrossRef]
13. Zhang, J.; Xu, H.; Li, W. High-purity CO_x-free H_2 generation from NH_3 via the ultra permeable and highly selective Pd membranes. *J. Membr. Sci.* **2006**, *277*, 85–93. [CrossRef]
14. Chellappa, A.; Fischer, C.; Thomson, W. Ammonia decomposition kinetics over Ni-Pt/Al_2O_3 for PEM fuel cell applications. *Appl. Catal. A Gen.* **2002**, *227*, 231–240. [CrossRef]

15. Le, T.A.; Kim, Y.; Kim, H.W.; Lee, S.-U.; Kim, J.-R.; Kim, T.-W.; Lee, Y.-J.; Chae, H.-J. Ru-supported lanthania-ceria composite as an efficient catalyst for COx-free H_2 production from ammonia decomposition. *Appl. Catal. B Environ.* **2021**, *285*, 119831. [CrossRef]
16. Staffell, I.; Scamman, D.; Velazquez Abad, A.; Balcombe, P.; Dodds, P.E.; Ekins, P.; Shah, N.; Ward, K.R. The role of hydrogen and fuel cells in the global energy system. *Energy Environ. Sci.* **2019**, *12*, 463–491. [CrossRef]
17. Yin, S.; Xu, B.; Zhou, X.; Au, C. A mini-review on ammonia decomposition catalysts for on-site generation of hydrogen for fuel cell applications. *Appl. Catal. A Gen.* **2004**, *277*, 1–9. [CrossRef]
18. Cha, J.; Jo, Y.S.; Jeong, H.; Han, J.; Nam, S.W.; Song, K.H.; Yoon, C.W. Ammonia as an efficient COX-free hydrogen carrier: Fundamentals and feasibility analyses for fuel cell applications. *Appl. Energy* **2018**, *224*, 194–204. [CrossRef]
19. Sørensen, R.Z.; Nielsen, L.J.; Jensen, S.; Hansen, O.; Johannessen, T.; Quaade, U.; Christensen, C.H. Catalytic ammonia decomposition: Miniaturized production of COx-free hydrogen for fuel cells. *Catal. Commun.* **2005**, *6*, 229–232. [CrossRef]
20. Valera-Medina, A.; Amer-Hatem, F.; Azad, A.K.; Dedoussi, I.C.; de Joannon, M.; Fernandes, R.X.; Glarborg, P.; Hashemi, H.; He, X.; Mashruk, S.; et al. Review on Ammonia as a Potential Fuel: From Synthesis to Economics. *Energy Fuels* **2021**, *35*, 6964–7029. [CrossRef]
21. Morlanés, N.; Katikaneni, S.P.; Paglieri, S.N.; Harale, A.; Solami, B.; Sarathy, S.M.; Gascon, J. A technological roadmap to the ammonia energy economy: Current state and missing technologies. *Chem. Eng. J.* **2021**, *408*, 127310. [CrossRef]
22. Zhang, Z.; Liguori, S.; Fuerst, T.F.; Way, J.D.; Wolden, C.A. Efficient Ammonia Decomposition in a Catalytic Membrane Reactor To Enable Hydrogen Storage and Utilization. *ACS Sustain. Chem. Eng.* **2019**, *7*, 5975–5985. [CrossRef]
23. Itoh, N.; Oshima, A.; Suga, E.; Sato, T. Kinetic enhancement of ammonia decomposition as a chemical hydrogen carrier in palladium membrane reactor. *Catal. Today* **2014**, *236*, 70–76. [CrossRef]
24. Itoh, N.; Kikuchi, Y.; Furusawa, T.; Sato, T. Tube-wall catalytic membrane reactor for hydrogen production by low-temperature ammonia decomposition. *Int. J. Hydrogen Energy* **2020**, *46*, 20257–20265. [CrossRef]
25. Cechetto, V.; Di Felice, L.; Martinez, R.G.; Plazaola, A.A.; Gallucci, F. Ultra-pure hydrogen production via ammonia decomposition in a catalytic membrane reactor. *Int. J. Hydrogen Energy* **2022**, *47*, 21220–21230. [CrossRef]
26. Cechetto, V.; Di Felice, L.; Medrano, J.A.; Makhloufi, C.; Zuniga, J.; Gallucci, F. H_2 production via ammonia decomposition in a catalytic membrane reactor. *Fuel Process. Technol.* **2021**, *216*, 106772. [CrossRef]
27. Cechetto, V.; Agnolin, S.; Di Felice, L.; Tanaka, A.P.; Tanco, M.L.; Gallucci, F. Metallic Supported Pd-Ag Membranes for Simultaneous Ammonia Decomposition and H_2 Separation in a Membrane Reactor: Experimental Proof of Concept. *Catalysts* **2023**, *13*, 920. [CrossRef]
28. Rizzuto, E.; Palange, P.; Del Prete, Z. Characterization of an ammonia decomposition process by means of a multifunctional catalytic membrane reactor. *Int. J. Hydrogen Energy* **2014**, *39*, 11403–11410. [CrossRef]
29. Israni, S.H.; Nair, B.K.R.; Harold, M.P. Hydrogen generation and purification in a composite Pd hollow fiber membrane reactor: Experiments and modeling. *Catal. Today* **2009**, *139*, 299–311. [CrossRef]
30. Li, G.; Kanezashi, M.; Lee, H.R.; Maeda, M.; Yoshioka, T.; Tsuru, T. Preparation of a novel bimodal catalytic membrane reactor and its application to ammonia decomposition for COx-free hydrogen production. *Int. J. Hydrogen Energy* **2012**, *37*, 12105–12113. [CrossRef]
31. Park, Y.; Cha, J.; Oh, H.-T.; Lee, T.; Lee, S.H.; Park, M.G.; Jeong, H.; Kim, Y.; Sohn, H.; Nam, S.W.; et al. A catalytic composite membrane reactor system for hydrogen production from ammonia using steam as a sweep gas. *J. Membr. Sci.* **2020**, *614*, 118483. [CrossRef]
32. Jo, Y.S.; Cha, J.; Lee, C.H.; Jeong, H.; Yoon, C.W.; Nam, S.W.; Han, J. A viable membrane reactor option for sustainable hydrogen production from ammonia. *J. Power Sources* **2018**, *400*, 518–526. [CrossRef]
33. Liu, J.; Ju, X.; Tang, C.; Liu, L.; Li, H.; Chen, P. High performance stainless-steel supported Pd membranes with a finger-like and gap structure and its application in NH_3 decomposition membrane reactor. *Chem. Eng. J.* **2020**, *388*, 124245. [CrossRef]
34. Jiang, J.; Dong, Q.; McCullough, K.; Lauterbach, J.; Li, S.; Yu, M. Novel hollow fiber membrane reactor for high purity H_2 generation from thermal catalytic NH_3 decomposition. *J. Membr. Sci.* **2021**, *629*, 119281. [CrossRef]
35. Cerrillo, J.L.; Morlanés, N.; Kulkarni, S.R.; Realpe, N.; Ramírez, A.; Katikaneni, S.P.; Paglieri, S.N.; Lee, K.; Harale, A.; Solami, B.; et al. High purity, self-sustained, pressurized hydrogen production from ammonia in a catalytic membrane reactor. *Chem. Eng. J.* **2021**, *431*, 134310. [CrossRef]
36. Kim, T.-W.; Lee, E.-H.; Byun, S.; Seo, D.-W.; Hwang, H.-J.; Yoon, H.-C.; Kim, H.; Ryi, S.-K. Highly selective Pd composite membrane on porous metal support for high-purity hydrogen production through effective ammonia decomposition. *Energy* **2022**, *260*, 125209. [CrossRef]
37. Sitar, R.; Shah, J.; Zhang, Z.; Wikoff, H.; Way, J.D.; Wolden, C.A. Compact ammonia reforming at low temperature using catalytic membrane reactors. *J. Membr. Sci.* **2022**, *644*, 120147. [CrossRef]
38. Omata, K.; Sato, K.; Nagaoka, K.; Yukawa, H.; Matsumoto, Y.; Nambu, T. Direct high-purity hydrogen production from ammonia by using a membrane reactor combining V-10mol%Fe hydrogen permeable alloy membrane with $Ru/Cs_2O/Pr_6O_{11}$ ammonia decomposition catalyst. *Int. J. Hydrogen Energy* **2022**, *47*, 8372–8381. [CrossRef]
39. *ISO 14687:2019*; Hydrogen Fuel Quality—Product Specification. International Organization for Standardization: Geneva, Switzerland, 2019.

40. Rahimalimamaghani, A.; Tanaka, D.P.; Tanco, M.L.; D'Angelo, F.N.; Gallucci, F. Effect of aluminium acetyl acetonate on the hydrogen and nitrogen permeation of carbon molecular sieves membranes. *Int. J. Hydrogen Energy* **2022**, *47*, 14570–14579. [CrossRef]
41. Rahimalimamaghani, A.; Tanaka, D.A.P.; Tanco, M.A.L.; D'angelo, M.F.N.; Gallucci, F. Ultra-Selective CMSMs Derived from Resorcinol-Formaldehyde Resin for CO_2 Separation. *Membranes* **2022**, *12*, 847. [CrossRef]
42. Gilron, J.; Soffer, A. Knudsen diffusion in microporous carbon membranes with molecular sieving character. *J. Membr. Sci.* **2002**, *209*, 339–352. [CrossRef]
43. Tanco, M.A.L.; Tanaka, D.A.P.; Rodrigues, S.C.; Texeira, M.; Mendes, A. Composite-alumina-carbon molecular sieve membranes prepared from novolac resin and boehmite. Part I: Preparation, characterization and gas permeation studies. *Int. J. Hydrogen Energy* **2015**, *40*, 5653–5663. [CrossRef]
44. Tanco, M.A.L.; Medrano, J.A.; Cechetto, V.; Gallucci, F.; Tanaka, D.A.P. Hydrogen permeation studies of composite supported alumina-carbon molecular sieves membranes: Separation of diluted hydrogen from mixtures with methane. *Int. J. Hydrogen Energy* **2021**, *46*, 19758–19767. [CrossRef]
45. Medrano, J.A.; Llosa-Tanco, M.A.; Cechetto, V.; Pacheco-Tanaka, D.A.; Gallucci, F. Upgrading biogas with novel composite carbon molecular sieve (CCMS) membranes: Experimental and techno-economic assessment. *Chem. Eng. J.* **2020**, *394*, 124957. [CrossRef]
46. Suda, H.; Haraya, K. Gas Permeation through Micropores of Carbon Molecular Sieve Membranes Derived from Kapton Polyimide. *J. Phys. Chem. B* **1997**, *101*, 3988–3994. [CrossRef]
47. Nordio, M.; Melendez, J.; Annaland, M.v.S.; Tanaka, D.A.P.; Tanco, M.L.; Gallucci, F. Comparison between carbon molecular sieve and Pd-Ag membranes in H2-CH4 separation at high pressure. *Int. J. Hydrogen Energy* **2020**, *45*, 28876–28892. [CrossRef]
48. Choudhary, T.; Sivadinarayana, C.; Goodman, D. Catalytic ammonia decomposition: COx-free hydrogen production for fuel cell applications. *Catal. Lett.* **2001**, *72*, 197–201. [CrossRef]
49. Chellappa, A.S.; Powell, M.R.; Fountain, M.; Call, C.J.; Godshall, N.A. Compact fuel processors for PEM fuel cells. *Fuel* **2002**, *10000*, 12000.
50. Alagharu, V.; Palanki, S.; West, K.N. Analysis of ammonia decomposition reactor to generate hydrogen for fuel cell applications. *J. Power Sources* **2010**, *195*, 829–833. [CrossRef]
51. Luna, B.; Somi, G.; Winchester, J.; Grose, J.; Mulloth, L.; Perry, J. Evaluation of Commercial Off-the-Shelf Sorbents & Catalysts for Control of Ammonia and Carbon Monoxide. In Proceedings of the 40th International Conference on Environmental Systems, Barcelona, Spain, 11–15 July 2010; International Conference on Environmental Systems (ICES). American Institute of Aeronautics and Astronautics: Reston, VA, USA, 2010. [CrossRef]
52. Huang, P.; Xu, N.; Shi, J.; Lin, Y. Characterization of asymmetric ceramic membranes by modified permporometry. *J. Membr. Sci.* **1996**, *116*, 301–305. [CrossRef]
53. Tsuru, T.; Hino, T.; Yoshioka, T.; Asaeda, M. Permporometry characterization of microporous ceramic membranes. *J. Membr. Sci.* **2001**, *186*, 257–265. [CrossRef]
54. Nakao, S.-I. Determination of pore size and pore size distribution: 3. Filtration membranes. *J. Membr. Sci.* **1994**, *96*, 131–165. [CrossRef]
55. Krantz, W.B.; Greenberg, A.R.; Kujundzic, E.; Yeo, A.; Hosseini, S.S. Evapoporometry: A novel technique for determining the pore-size distribution of membranes. *J. Membr. Sci.* **2013**, *438*, 153–166. [CrossRef]

Disclaimer/Publisher's Note: The statements, opinions and data contained in all publications are solely those of the individual author(s) and contributor(s) and not of MDPI and/or the editor(s). MDPI and/or the editor(s) disclaim responsibility for any injury to people or property resulting from any ideas, methods, instructions or products referred to in the content.